ELSEVIER

Contents lists available at ScienceDirect

# Sustainable Cities and Society

journal homepage: www.elsevier.com/locate/scs





# WebMRT: An online tool to predict summertime mean radiant temperature using machine learning

Saud R. AlKhaled a,\*, Ariane Middel b, Pouya Shaeri c, Isaac Buo d, Florian A. Schneider e

- <sup>a</sup> College of Architecture, Kuwait University, Adailiya, Kuwait
- b School of Arts, Media and Engineering (AME), School of Computing and Augmented Intelligence (SCAI), Arizona State University, United States
- <sup>c</sup> School of Computing and Augmented Intelligence (SCAI), Arizona State University, United States
- d Luskin Center for Innovation, School of Public Affairs, University of California, Los Angeles, United States
- e Climate and Energy Program (CEP), Third Way, United States

#### ARTICLE INFO

#### Keywords: Urban climate Heat stress Mean radiant temperature LightGBM SAM Empirical model

#### ABSTRACT

Mean Radiant Temperature ( $T_{mrt}$ ) is the most critical atmospheric variable influencing outdoor human thermal exposure and comfort in hot, dry environments. However, accurately quantifying  $T_{mrt}$  requires time-consuming field measurements with expensive equipment or complex, resource-intensive computations. We introduce WebMRT, an online tool to predict  $T_{mrt}$  using a data-driven approach. It features an intuitive interface using air temperature, shading status, and built environment features as predictors of  $T_{mrt}$  for a user-selected summer day, time, and location. Utilizing a tree-based ensemble model, WebMRT is trained on state-of-the-art human-biometeorological data collected by MaRTy using LightGBM after evaluating its performance against several candidate machine learning regressors. Feature engineering was applied to the day and time input, and two additional temporal features were derived: 'Solar Altitude' and 'Minutes-from-Sunrise'. These inputs are integrated into the user interface, emphasizing simplicity and easy access for users at the frontend. After training the regressor on MaRTy datasets and employing k-fold cross-validation with ten folds, the model demonstrated strong predictive power (R²=0.92) with acceptable error (RMSE=3.43, MAPE=5.33) and bias (MBE=0.20). WebMRT also features optional fisheye photo uploads, processed using transfer learning techniques for image segmentation, further enhancing the tool's predictive accuracy, user experience, and applications towards climate action decision-making processes.

#### 1. Introduction

Outdoor human thermal exposure is a pressing public health concern, particularly in rapidly growing desert cities where vulnerability to extreme heat is already intensified by global climate change (IPCC, 2023). Identifying conditions that lead to thermal stress requires several micrometeorological factors beyond air temperature, including shortwave and longwave radiation, wind speed, and humidity (Guzman-Echavarria, Middel & Vanos, 2023). During extreme heat events, wind speed is usually low, diminishing the effectiveness of convective cooling. In such situations, radiation becomes the primary factor influencing thermal comfort and stress, particularly in hot and dry climates (Lindberg, Holmer & Thorsson, 2008; Middel, AlKhaled, Schneider, Hagen & Coseo, 2021; Shashua-Bar, Pearlmutter & Erell,

2011). Given these conditions, mean Radiant Temperature ( $T_{mrt}$ ) has been recognized as the most critical atmospheric metric influencing the human thermal experience (Guo et al., 2020; Johansson, Thorsson, Emmanuel & Krüger, 2014; Thorsson, Lindberg, Eliasson & Holmer, 2007).  $T_{mrt}$  summarizes the effects of short and longwave fluxes (direct and reflected) on the human body and is an essential indicator of thermal exposure in human biometeorology. In current research and practice,  $T_{mrt}$  has been widely used as a crucial variable for thermophysiological stress indices such as UTCI (Jendritzky, de Dear & Havenith, 2012), PET (Höppe, 1999), and SET\* (Gagge, Fobelets & Berglund, 1986). However, calculating  $T_{mrt}$  is complex, and predicting it presents several challenges, including the need for field measurements and the computational complexities involved.

Various methods exist to obtain  $T_{mrt}$  from field measurements and

E-mail addresses: saud.alkhaled@ku.edu.kw (S.R. AlKhaled), ariane.middel@asu.edu (A. Middel), pshaeri@asu.edu (P. Shaeri), ibuo@luskin.ucla.edu (I. Buo), fschneider@thirdway.org (F.A. Schneider).

https://doi.org/10.1016/j.scs.2024.105861

<sup>\*</sup> Corresponding author.

numerical modeling (Kántor & Unger, 2011). Field measurements range from complex setups using pyranometers and pyrgeometers oriented in six directions to simpler, though less accurate, infrared camera (Merchant et al., 2022; Middel, Huff, Krayenhoff, Udupa & Schneider, 2023), globe thermometer (Krüger, Minella & Matzarakis, 2014), and cylindrical thermometer methods (Rykaczewski et al., 2024). The impact of the different measurement approaches on  $T_{mrt}$  values has been the focus of several studies (Thorsson et al., 2007; Vanos et al., 2021). Often, such measurements are unavailable or lack the temporal continuity necessary for urban planning and design decision-making processes.

Longitudinal studies have relied on numerical modeling to simulate Tmrt, using parameterized models such as RayMan (Matzarakis, Rutz & Mayer, 2007) and SOLWEIG (Lindberg et al., 2008), as well as computational fluid dynamic models like ENVI-met (Bruse & Fleer, 1998). However, these models encounter several challenges, including: (a) inadequate physical process modeling, particularly in the calculation and reflection of surface temperatures; (b) limited support for vector data formats, which restricts the integration of detailed geographic data essential for accurate modeling; and (c) high computational demands (Buo, Sagris, Jaagus & Middel, 2023; Gál & Kántor, 2020; Wu, Fang, Liu

& Middel, 2023). Consequently, the oversimplified representations inherent to these models often compromise  $T_{mrt}$  predictions and limit their effectiveness in routine decision-making processes.

Recognizing these challenges, this study introduces WebMRT, an online tool to predict  $T_{mrt}$  using machine learning models trained on state-of-the-art T<sub>mrt</sub> measurements and built environment features (360degree surface type fractions) collected in the Desert Southwest US using MaRTy (Middel et al., forthcoming; Middel & Krayenhoff, 2019). The primary objective of WebMRT is to bridge the gap in current methodologies, which typically rely on complex field observations and intensive computational resources to predict  $T_{mrt}$ . WebMRT offers a streamlined alternative by using empirical models that provide accurate predictions without the extensive computational demands of numerical modeling. The simplicity of WebMRT's user interface enhances its accessibility, making it particularly engaging for stakeholders and policy officials. This interface, combined with the tool's ability to integrate and process data efficiently, supports timely and decision-making in urban heat stress mitigation. Consequently, WebMRT contributes to data-driven urban climate governance, a need underscored by recent studies such as those by Hughes, Giest and Tozer (2020) and Middel, Nazarian, Demuzere and Bechtel (2022).

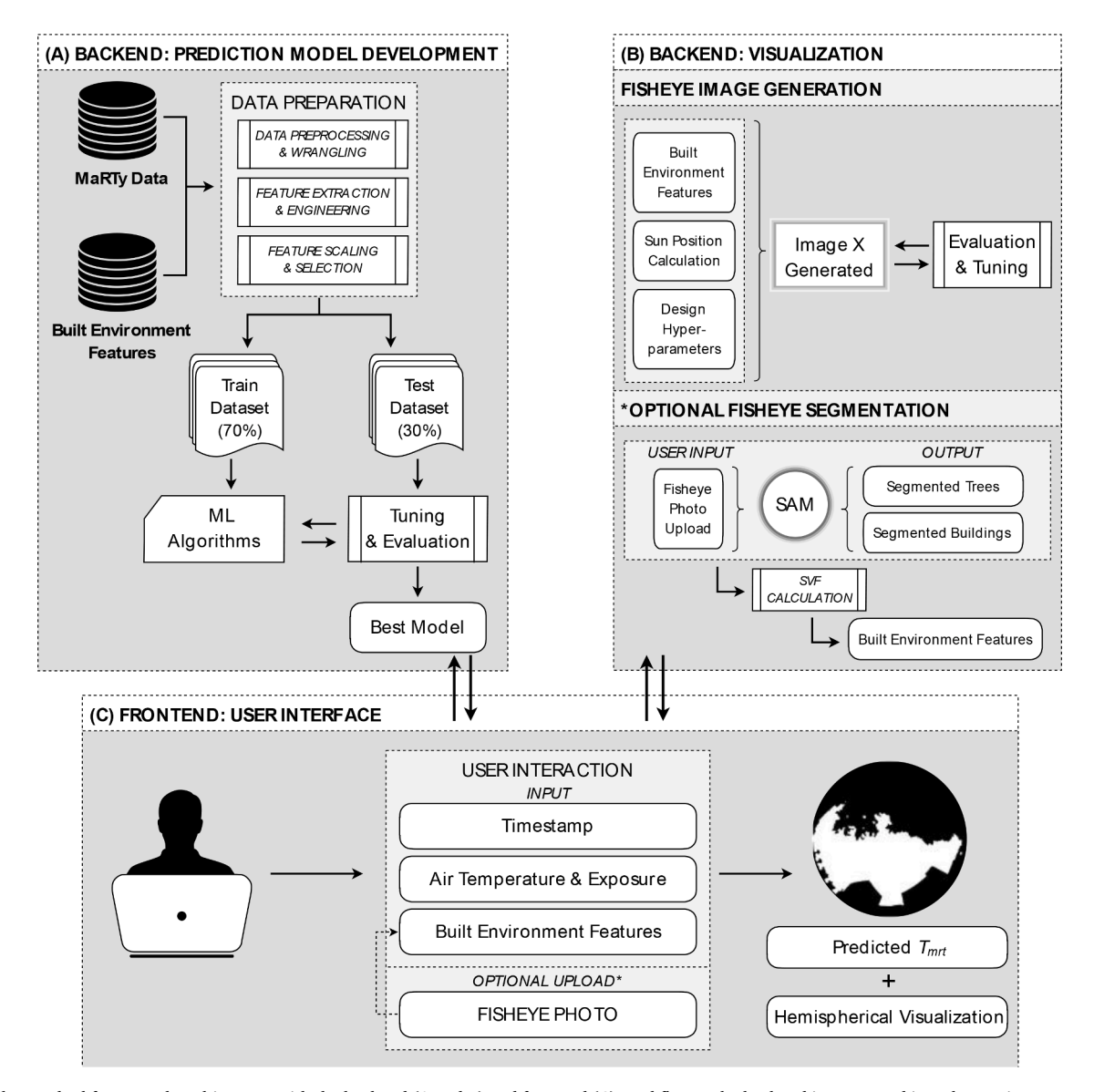


Fig. 1. WebMRT dual framework architecture with the backend (A and B) and frontend (C) workflows. The backend is structured into three primary components: the  $T_{mrt}$  Prediction Model, the Fisheye (Hemispherical) Image Generator, and the Fisheye Segmentation Model.

The remainder of this paper is organized as follows: Section 2, details the techniques and processes used in the development of WebMRT, from data sourcing to the overarching web application architecture. Section 3 presents the rationale behind selecting the prediction model, its performance compared to other machine learning regressors, and the functionality of WebMRT's user interface. Section 4 considers the implications and potentials of WebMRT for broader engagement among stakeholders. Finally, the paper concludes with Section 5 which outlines the significance of WebMRT and future research directions.

#### 2. Materials and methods

The development of WebMRT involved various tasks, from data sourcing and backend model development to photo segmentation and the design of a user-friendly interface (Fig. 1). All dataset management tasks were performed using R (Version 4.2.1). Python (Version 3.10) was utilized for machine learning using the *Scikit-learn* library (Pedregosa et al., 2011). The interface of WebMRT was developed in HTML, CSS, and JavaScript.

#### 2.1. Data sources

The empirical model in the WebMRT backend is based on MaRTy human-biometeorological measurements in the Phoenix metropolitan area (Middel & Krayenhoff, 2019; Middel et al., 2021), alongside built environment features derived from hemispherical fisheye photographs (Middel, Lukasczyk, Zakrzewski, Arnold & Maciejewski, 2019).

The Phoenix metropolitan area is the largest city in the Sonoran Desert and classified under the Köppen-Geiger climate type BWh, indicative of a hot, arid desert (Kottek, Grieser, Beck, Rudolf & Rubel, 2006). During the summer months of June, July, and August, the region typically experiences dry conditions and intense heat, with average daily maximum air temperatures exceeding 40 °C for the 1991–2020 period. The monsoon season, which extends from June 15 to September 30, introduces higher humidity levels. Throughout May to September, the average nightly minimum air temperature remains well above 20 °C.

The human-biometeorological dataset, a gold standard in the field, includes hourly measurements of air temperature, humidity, wind speed, and six-directional shortwave and longwave radiation (Middel et al., forthcoming). These measurements were recorded using the MaRTy mobile human-biometeorological station across various sites and summertime days in the Desert Southwest USA between 2016 and 2019.  $T_{mrt}$  is calculated using the six-directional method, with three-dimensional radiation budgets decomposed into directional weighted components of shortwave and longwave radiation.  $T_{mrt}$  observations for each site are coupled with view factors of built environment features, calculated from image cubes, to determine the main drivers of  $T_{mrt}$  and thermal exposure. Those include percent sky, trees, buildings, impervious surfaces, pervious surfaces, and non-permanent objects. A detailed description of MaRTy and the methodology behind calculating view factors of built environment features are available in Middel and Krayenhoff (2019) and Middel et al. (2021).

#### 2.2. Backend development

#### 2.2.1. Empirical model development

WebMRT's backend prediction model follows the main steps of a typical machine learning workflow. It consists of (1) data preparation, (2) data splitting into training and testing subsets, (3) identifying candidate algorithms, (4) model training and tuning, and (5) model performance evaluation and comparison.

2.2.1.1. Data preparation. A dataset was compiled to estimate  $T_{mrt}$  using various built environment features as predictor variables for entry into the machine learning process. As discussed in Section 2.1, two datasets

were merged: the MaRTy dataset containing  $T_{mrt}$  values along with observation metadata, and the dataset detailing built environment view factors, categorized into six classes of potential predictor variables—sky, trees, buildings, impervious surfaces, pervious surfaces, and non-permanent objects— considering both spatial and temporal factors. During data preprocessing and wrangling, missing values were removed, and categorical variables were converted to a numerical format as necessary through one-hot encoding. Descriptive statistics of the merged dataset are reported in Table 1.

In the feature engineering phase, additional variables pertinent to solar radiation were derived using R's suntools package (Bivand et al., 2023) and incorporated into the dataset. Specifically, the solar position (altitude) and time (minutes from sunrise) were determined from each measurement's geographic coordinates and timestamp. These features are crucial as they normalize solar position and exposure time, enhancing accuracy beyond what a timestamp alone can offer. This normalization is especially relevant to  $T_{mrt}$  predictions, improving the model's ability to accurately represent thermal conditions. The selection of features, including extracted and engineered variables, was determined through backward elimination and feature importance ranking. The final set of selected features included: (1) air temperature, (2) solar altitude, (3) minutes from sunrise, (4) shade at measurement, and the view factors of surrounding (5) sky, (6) buildings, (7) trees, and (8) pervious ground cover.

2.2.1.2. Training and testing subsets. The dataset was split into training and testing subsets. 70% of the data was allocated for training, while the remaining 30% was set aside for testing. In addition to the validation processes (Section 2.2.1.4), a predetermined random seed was utilized to maintain consistency and reproducibility in the data division. Following the data split, the training and testing subset indices, encompassing the features and the target variable, were reset. This procedure ensures that the data's structural integrity is preserved throughout the machine-learning process, particularly when cross-validation techniques are implemented (Section 2.2.1.4).

2.2.1.3. Identifying candidate algorithms. The candidate algorithm selection was driven by the necessity to examine a range of modeling techniques capable of handling the complex relationships and varied data types in the dataset. Simple linear models such as Ridge (Hoerl & Kennard, 1970) and Lasso Regression (Tibshirani, 1996) were included because they address multicollinearity and feature selection. Kernel-based methods like Support Vector Regression (Smola & Schölkopf, 2004) were selected for their capacity to handle non-linear relationships through different kernel functions. Advanced tree-based ensemble methods including Decision Tree (Loh, 2011), Random Forest (Breiman, 2001), LightGBM (Ke et al., 2017), and XGBoost (Chen & Guestrin, 2016) were chosen for their robustness and high performance in capturing complex data structures while preventing overfitting, which is critical for achieving the predictive accuracy objectives of WebMRT. The rationale behind each selection relates directly to the algorithm's known strengths and alignment with the specific challenges presented by the dataset characteristics, ensuring a comprehensive evaluation of different approaches. The objective was to identify the most effective algorithm that would exhibit superior predictive accuracy across the various models.

2.2.1.4. Model tuning and evaluation. Tuning refers to the process of

**Table 1**Dataset description.

No. of observations:	2159	Hours:	0730-2030
No. of features:	12	Months:	June - August
Data types:	Numeric & Nominal	$T_{air}$ ( °C):	26.02-43.97
Years:	2016; 2018- 2019	$T_{mrt}$ ( $^{\circ}$ C):	15.54-76.22

adjusting the hyperparameters of the models to improve performance. The hyperparameter space is preset before the learning process to modify the learning structure and process but is not derived from the data per se. It involves identifying the optimal settings within the predefined space through an iterative process of testing various combinations and assessing their impact on the model's predictive power.

The selection of hyperparameters for tuning was informed by the known sensitivities and performance impacts associated with each model type. For linear and kernel-based models, an exhaustive grid search approach was employed to systematically explore combinations of parameters and ascertain the most effective settings. In contrast, due to the vast hyperparameter space of tree-based ensemble models, a randomized search strategy was adopted, enabling the efficient identification of high-performing configurations without the need for exhaustive testing. To mitigate the risks of overfitting and ensure the reliability of the tuning results, a 10-fold cross-validation approach was employed (James, Witten, Hastie & Tibshirani, 2013). In every tuning iteration, nine folds were used for the training of the model, and the remaining one-fold was used for validation. The assessment of the hyperparameter settings was based on averaging the performance metrics from these ten validations.

After the tuning process, the predictive capabilities and accuracy of all models were evaluated. Table 2 presents the four performance metrics used for evaluating the models: the coefficient of determination ( $\mathbb{R}^2$ ), which indicates how well the model's predictions match the variance of the data; Root Mean Square Error (RMSE), measuring the average prediction error magnitude; Mean Bias Error (MBE), indicating the average prediction bias; and Mean Absolute Percent Error (MAPE), assessing the average percentage error relative to actual values. These metrics collectively provide insights into the accuracy and efficacy of the models by quantifying the deviation of model predictions from observed  $T_{mrt}$  values.

#### 2.2.2. Fisheye image processing

2.2.2.1. Fisheye (Hemispherical) image generation. A JavaScript-based model was developed to dynamically generate a hypothetical fisheye image that displays the simulated hemispherical view corresponding to the built environment features and exposure conditions selected by the user in real time (Fig. 2). Digital representations of buildings, trees, and sky textures (daytime, nighttime, and sun vector images) were used as individual elements for the hypothetical view. Driven by user inputs, the model dynamically composes a panoramic scene on an HTML canvas element. A stereographic projection is applied to the panorama, with fine-tuning hyperparameters to adjust size, randomness, overlay ratio, and distance from the border to enhance the simulation's resemblance to real-world conditions. The validation and optimization of these hyperparameters were iteratively conducted through the segmentation of output images and their subsequent comparison with user inputs. Finally, the SunCalc library (Agafonkin, 2023) was used to calculate the sun's position for accurate dynamic solar exposure and trajectory

**Table 2** Model performance evaluation metrics.

Metric	Equation
Coefficient of determination	$R^2 = 1 - rac{\sum_{i=1}^{n} \left( y_i - f(x_i)  ight)^2}{\sum_{i=1}^{n} \left( y_i - \overline{y}  ight)^2}$
Root mean squared error	$RMSE = \sqrt{\frac{\sum_{i=1}^{n} (f(x_i) - y_i)^2}{n}}$
Mean bias error	$MBE = \frac{\sum_{i=1}^{n} (f(x_i) - y_i)}{n}$
Mean absolute percent error	MAPE $=\frac{100}{n}\sum_{i=1}^{n} \frac{y_{i}-f(x_{i})}{y_{i}} $

 $y_i$  represents the i<sup>th</sup> observed value and  $f(x_i)$  represents the i<sup>th</sup> predicted. value for a total of n observations, and  $\bar{y}$  is the mean of all observations.

simulation. If enabled by the user, the sun's trajectory is optionally visualized by rendering a sun path diagram.

2.2.2.2. Fisheye segmentation using SAM. The primary purpose of processing a user-uploaded fisheye image is to eliminate the need for users to know the surrounding built environment feature composition and apply the model to real-world locations. Fisheye photos are processed in three steps: (a) image preprocessing and advanced image segmentation (SAM); (b) Sky View Factor (SVF) calculation; and (c) extraction and quantification of the relevant features. Upon uploading, the image is first resized and converted into a standard format appropriate for the subsequent processes using Python's pillow library (Clark, 2023). The urban environment, as depicted in the uploaded fisheye image, is analyzed using the Segment Anything Model (SAM). Trained on over 1 billion segmentation masks from Meta AI's Segment Anything project, SAM adapts to segmentation tasks using principles of transfer learning without the need for custom annotations or extensive retraining (Kirillov et al., 2023). Specifically, for WebMRT, SAM's task is to identify buildings and trees as specific features to compute their coverage ratios within the hemispherical scene. The image is then partitioned into annular rings where the SVF is calculated by summing up the contribution of each ring following Middel, Lukasczyk and Maciejewski (2017) adapted version of the manual Steyn method (Chapman, Thornes & Bradley, 2001).

#### 2.3. Frontend development

#### 2.3.1. User interface design

The user interface was designed in HTML and CSS. A noteworthy dynamic element is the custom-made ternary slider, consisting of a triangle image with a draggable circle (Fig. 3). Moving the circle within the triangle's borders allows users to adjust the proportions of the built environment features (*SVF*, *buildings*, and *trees*) while ensuring their cumulative proportions always complete a whole (100%).

The ternary slider is implemented in JavaScript, using the D3.js library (Bostock, Ogievetsky & Heer, 2011) for graphical manipulations and the jQuery library to streamline Document Object Model (DOM) interactions and event handling. The input controls determining the remaining predictor variables are dynamically handled through WebMRT's integration of AJAX for asynchronous server communication. It allows updating the  $T_{mrt}$  predictions and visualizations in real-time by enabling communication between the front and back end.

# 2.3.2. Web application architecture

WebMRT's framework architecture combines client-side interactivity and server-side computation (Fig. 4). Central to the application's architecture is a Flask server, which manages HTTP requests and the direction of information flow. Comprised of routes and views, the architecture facilitates processing incoming data and generating appropriate responses.

The SAM model and the SVF calculator (Section 2.2.2.2) run on the server. Upon receiving the user input (and the processed image data from the optional fisheye photo), the Flask server calculates solar altitude and minutes from sunrise as the two feature-engineered variables (Section 2.2.1.1), incorporating them with built environment features (SVF, buildings, and trees), surface characteristics (pervious ground cover), and exposure conditions (air temperature and shade at measurement) before they are fed into the machine learning model. Predicted  $T_{mrt}$  is then returned to the front end and displayed to the user.

The front end, constructed with HTML, CSS, and JavaScript, provides the interface for users to interact with WebMRT. It includes a ternary slider (Section 2.3.1) controlled by JavaScript event handlers, enabling users to input model feature variables manually. Fisheye images (Section 2.2.2) are generated with JavaScript, which simulates the built environment and exposure conditions determined by user inputs.

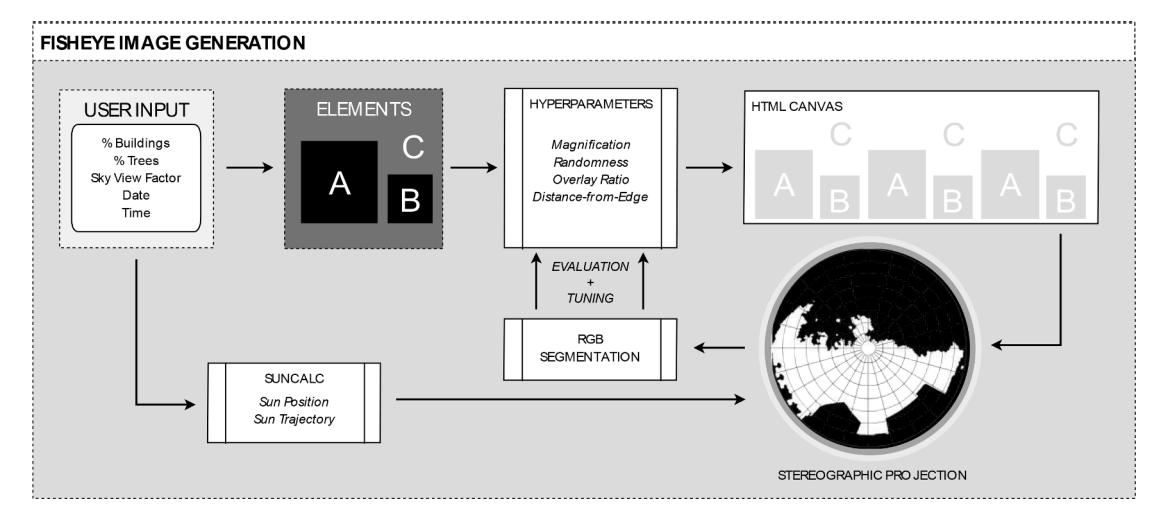
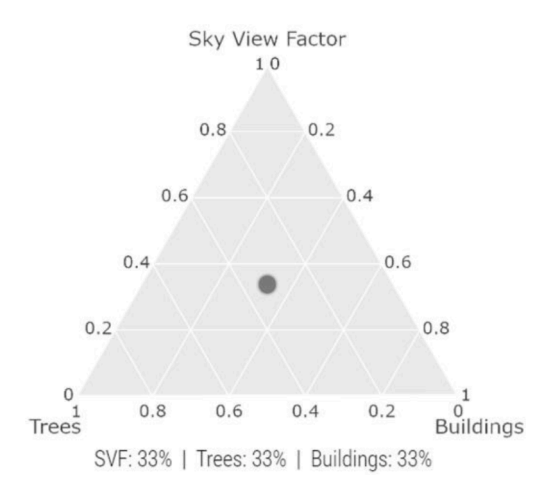


Fig. 2. Workflow of the fisheye (hemispherical) image generation.



**Fig. 3.** A ternary slider in the form of a triangle was developed as a control element to represent the built environment features ensuring their cumulative proportions always complete a whole. Each corner of the triangle represents one of the three inputs at its maximum value, and the user can determine the combination ratio by moving the circle within the triangle. The position of the circle determines the proportion of each feature within a given study area.

The application architecture thus encapsulates a bidirectional data flow between the front and back end. This includes the collection of user inputs via interactive web elements, the image processing logic in the front end, the predictive modeling in the backend, and the final delivery of  $T_{mrt}$  predictions to the user interface.

#### 3. Results

#### 3.1. Model performance

The results of the models' predictive power are reported in Table 3 and are further illustrated graphically as a Taylor Diagram in Fig. 5. LightGBM stands out as the top-performing model, closely followed by XGBoost, considering all evaluated performance metrics. The Random Forest model remains competitive, especially in error minimization and maintaining low bias as depicted by its position in relation to the concentric standard deviation arcs in the Taylor Diagram. The SVR and Decision Tree models can somewhat accurately predict and manage error sizes and percentages. However, compared to advanced tree-based ensembles, they exhibit error reduction and percentage error minimization limitations. Although the linear models perform adequately, they

do not match the tree-based models' precision and show larger discrepancies between predicted and actual values.

This comparative analysis indicates the strength of tree-based ensemble models, particularly LightGBM, emerging as the superior model when compared to XGBoost and Random Forest. One reason LightGBM excels is its use of gradient-based one-sided sampling, which filters out data instances with small gradients. This speeds up the learning process and improves model accuracy (Ke et al., 2017). Another feature is its leaf-wise growth strategy, in contrast to the level-wise growth strategy used by traditional models such as Random Forest. This approach allows for more complex decision boundaries, thereby improving LightGBM's ability to capture data complexities (Ke et al., 2017). These outcomes are clearly demonstrated in its high predictive power ( $R^2 = 0.915$ ) with acceptable error (RMSE = 3.436, MAPE = 5.331) and minimal bias (MBE = 0.198). These advancements in machine learning, as demonstrated in this analysis, have enabled models such as LightGBM to outperform traditional empirical methods, overcoming some of the diagnostic limitations with superior predictive accuracy and nuanced data complexity handling.

## 3.2. WebMRT user interface

Upon loading WebMRT (https://shadelab.asu.edu/webmrt/) the user interacts with the model via a web browser (Fig. 6), which is the entry point for required model input data. The interface is divided into several interactive components:

- Date and Time Selection: At the top left, users can select a specific date, with an adjacent time selector with an option to visualize the sun's trajectory.
- Ternary Slider for Built Environment Features: Below the date and time selection, a ternary slider is available where users can adjust the view fractions of "Sky", "Trees", and "Buildings" surrounding the study area of interest. For verification, the selected values are presented as a percentage below the diagram.
- Adjustable Sliders and Checkbox: To the right of the ternary slider, two number sliders are available for the user to set the "Percentage of Surrounding Pervious Area" and "Air Temperature." A checkbox is also available to indicate if the study area is sun-exposed or shaded.
- **Predicted**  $T_{mrt}$  **Display:** Below these controls, the predicted  $T_{mrt}$  value is displayed for the given conditions. Users can save their defined parameters and the corresponding  $T_{mrt}$  predictions as scenarios, which can be exported in CSV format.

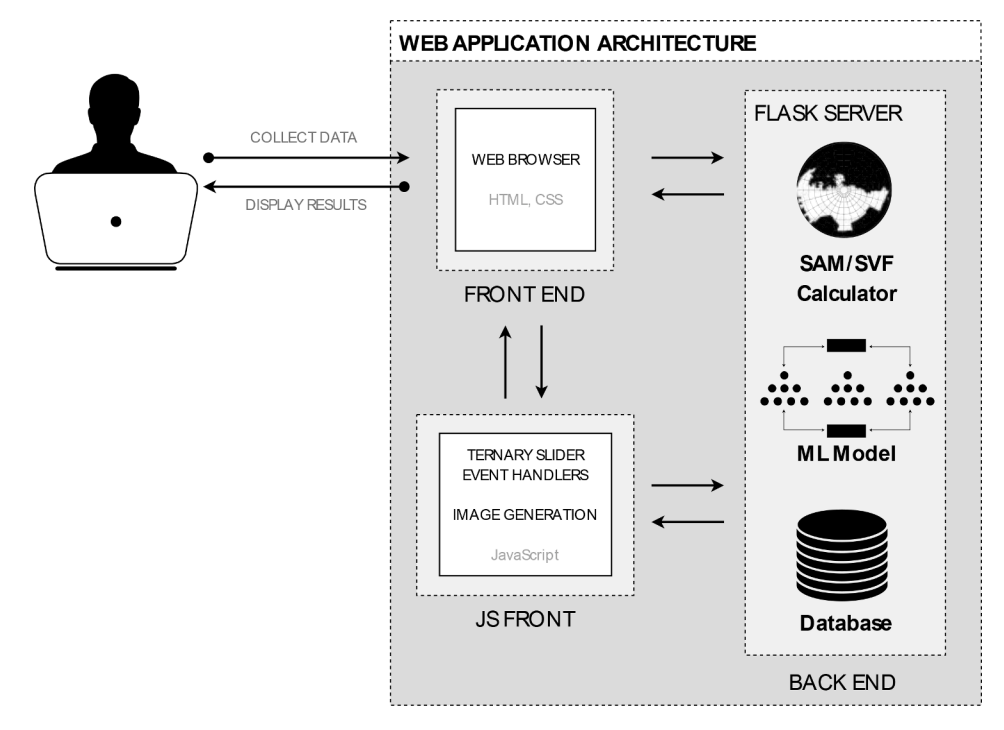


Fig. 4. Overview of WebMRT's framework architecture, schematically highlighting the interaction between the user, web browser, and additional front/backend services.

**Table 3**Prediction model performance on testing subset.

	R2	RMSE	MAPE	MBE
Linear				
Ridge	0.782	5.434	10.608	-0.226
Lasso	0.777	5.497	10.889	-0.219
Kernel-based				
SVR	0.884	3.962	5.941	-0.320
Tree-based Ensemble				
Decision Tree	0.836	4.714	7.540	0.158
Random Forrest	0.912	3.458	5.362	0.130
XGBoost	0.913	3.436	5.331	0.198
LightGBM	0.915	3.404	5.235	0.127

- **Fisheye Image:** To the right of the sliders, a fisheye (hemispherical) image is generated, simulating the built environment and exposure conditions as determined by user inputs.
- Upload Feature: Below the fisheye image, an optional upload feature is available to replace the manual input of built environment feature variables. The process button would adjust the draggable point in the ternary slider to represent the fractions of sky, trees, and buildings depicted in the uploaded image.
- Instructions Panel: To the right, a dedicated panel provides instructions on how to use the tool.

The user interface is designed to facilitate sequential navigation from input variables to the predicted  $T_{mrt}$  outcome, ensuring a user-friendly experience.

## 4. Discussion

WebMRT is designed as an accessible tool that enables stakeholders to make informed decisions on urban design and policy enhancements for improved outdoor thermal exposure and comfort. This objective was made possible by integrating AI-driven functionalities across machine learning and predictive analytics, deep learning generative AI, and computer vision.

Compared to other widely used microclimate numerical models such as RayMan, SOLWEIG, and ENVI-met, it is notable that WebMRT streamlines the modeling process. This feature allows users to configure the model to predict  $T_{mrt}$  without requiring extensive urban climate knowledge, thus saving time, and facilitating broader engagement among professionals and stakeholders in the decision-making process. This has significant implications for policy and science, making WebMRT accessible to a wider audience.

Importantly, WebMRT's simplicity does not compromise accuracy. While uncertainties in the predicted  $T_{mrt}$  for the other popular models are reported to be within the  $\pm 5$  °C threshold (Crank et al., 2020; Forouzandeh, 2018; Gál & Kántor, 2020; Krüger et al., 2014; Zhao & Fong, 2017), WebMRT maintains a tighter uncertainty of  $\pm 3.43$  °C. Additionally, WebMRT's streamlined process from input to prediction enables intricate sensitivity analysis and scenario comparisons, which are typically time-consuming in other numerical models. This efficiency not only expedites the decision-making process but also significantly contributes to making science actionable, addressing the science-policy communication gap as noted by Schneider, Epel and Middel (2024). This capability ensures that stakeholders can quickly evaluate different urban planning and design strategies, making informed decisions with high degrees of accuracy.

On the other hand, WebMRT has several limitations that warrant consideration. As an empirical model, it is inherently constrained by the dataset it utilizes. Firstly, the MaRTy Dataset is currently limited to the summer months of the Desert Southwest US and mainly includes day-time observations. Secondly, the selection of model input features, or predictor variables, is heavily influenced by that dataset and determined based on feature importance ranking. Consequently, in its current form, WebMRT may not fully account for variables that are critical to assessing outdoor thermal exposure and comfort during nighttime or in different climatic conditions.

However, it is important to note that observations in Phoenix are ongoing, and the database is expected to expand in the future to also cover nighttime predictions. Plans are also in place to include observations from other geographic locations that have MaRTy data, such as Singapore, Australia, and Canada. This expansion will enable WebMRT

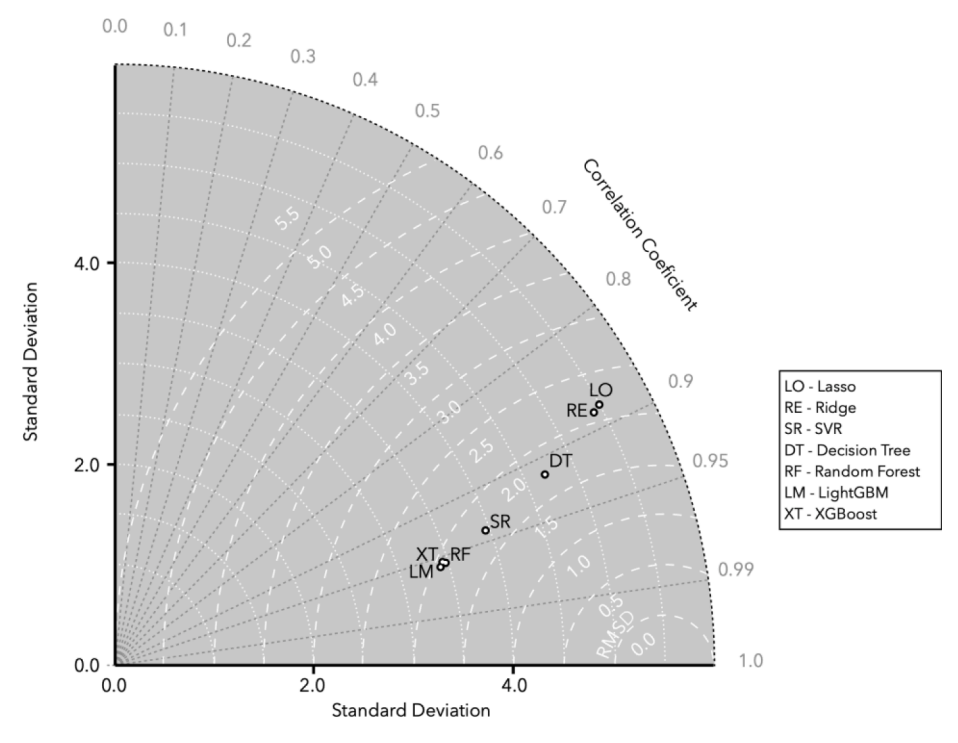


Fig. 5. Taylor Diagram visualizing the accuracy of the prediction models, with each model's performance depicted as a point. The angular position of each point indicates the correlation coefficient with the observations, the radial distance from the origin denotes the model predictions' standard deviation, and the concentric circles represent the normalized Root Mean Square Deviation (RMSD) from the observations.

to enhance its learning process and extend its prediction across a broader spectrum of environmental conditions, including diverse seasonal and nocturnal scenarios.

Lastly, the current version of WebMRT does not account for the cardinal direction of interventions, such as urban canyon orientations or tree clusters. This omission could limit the model's practicality in urban planning scenarios. Nevertheless, the workflow upon which WebMRT was designed offers many possibilities for future research to incorporate such parameters during the model's learning process, thereby extending its utility and applicability. Future enhancements may also include capabilities for users to access detailed feature importance metrics, enhancing transparency and understanding of the model's predictive dynamics.

#### 5. Conclusions

WebMRT was developed in direct response to the challenges of measuring and calculating  $T_{mrb}$  emphasizing simplicity for relevant stakeholders to make informed decisions for urban design and policy enhancement. It emerges not only as a practical tool for the Desert Southwest but also as a concept with the potential to be scaled across diverse climate regions. By integrating advanced datasets with machine learning algorithms and emphasizing a user-focused design, WebMRT is developed to offer a reliable predictive model and a straightforward interface. This approach aims to ensure accurate  $T_{mrt}$  predictions, making it accessible and easy to use for a wide range of users. As an empirical model, it aligns with the evolving paradigm of urban climate informatics (Middel et al., 2022) and data-driven urban climate governance outlined by Hughes et al. (2020). The structure of WebMRT is designed to accommodate open-source data integration, enabling its application beyond summertime in the Desert Southwest to encompass different climate regions and seasonal contexts. This flexibility showcases the potential of modern data science approaches in solving complex environmental challenges that previously relied heavily on resource-intensive, physics-based models. By leveraging faster, more efficient computational methods and larger, more diverse datasets,

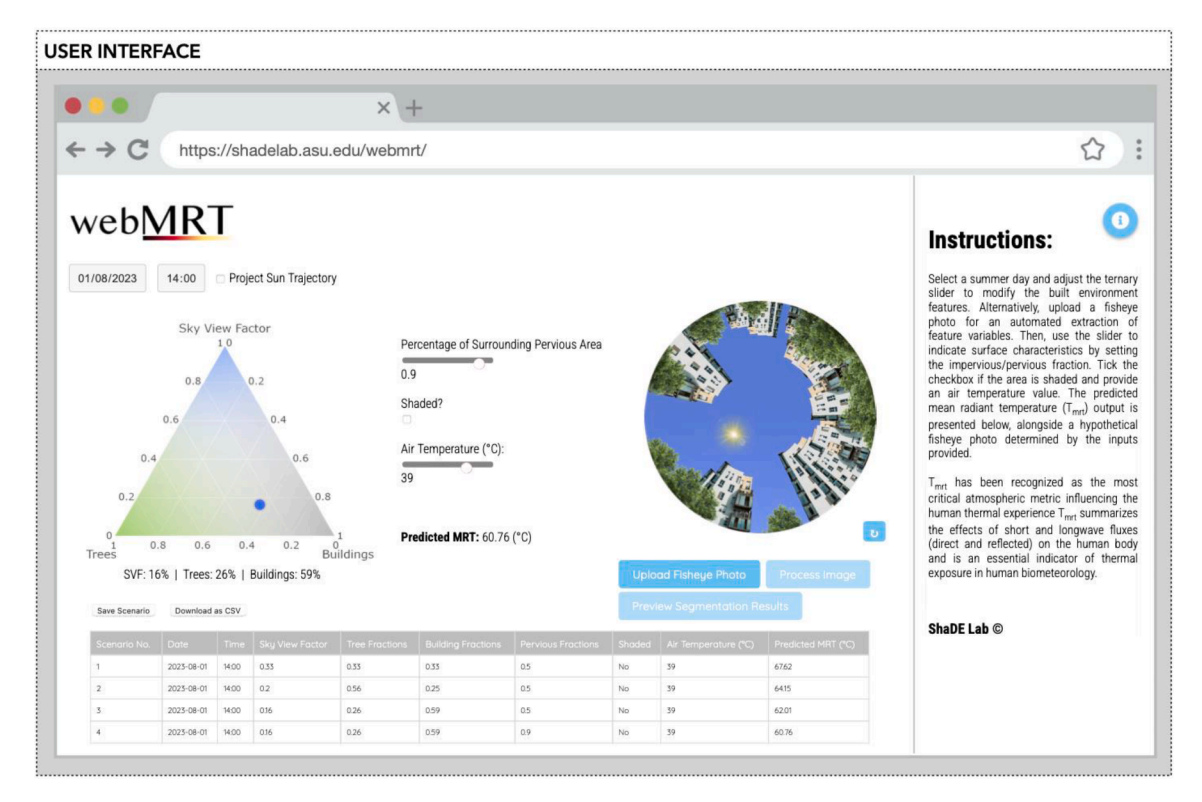
researchers and policymakers can achieve improved decision-making capabilities and enhanced predictive analytics, enabling deeper insights and more effective interventions.

Future developments of WebMRT and similar tools could further harness advancements in real-time data feeds and IoT devices to enhance the tool's predictive accuracy and usability. Specifically, integrating IoT sensors distributed across various locations would improve the data collection process and enable real-time or near-real-time predictive modeling. This integration could lead to more dynamic models that adjust predictions based new incoming data and retraining cycles. Moreover, the use of IoT technology could facilitate continuous updates to the model, improving predictive capabilities as more data becomes available and across varying conditions.

In addition to these enhancements, future versions of WebMRT could significantly benefit from improved interface functionality. For instance, linking WebMRT to a Weather API for forecasting would allow the tool to incorporate current and forecasted weather conditions into its predictions, providing users with more accurate and timely information. Furthermore, enabling users to select a location directly on a map to automatically generate a fisheye image could simplify user interactions and reduce the number of steps needed to obtain predictions. These interface enhancements would improve the user experience and extend the practical applications of WebMRT.

#### CRediT authorship contribution statement

Saud R. AlKhaled: Writing – review & editing, Writing – original draft, Visualization, Validation, Software, Methodology, Investigation, Formal analysis, Data curation, Conceptualization. Ariane Middel: Writing – review & editing, Validation, Resources, Methodology, Formal analysis, Data curation. Pouya Shaeri: Writing – review & editing, Visualization, Validation, Software, Methodology. Isaac Buo: Writing – review & editing, Validation, Methodology. Florian A. Schneider: Writing – review & editing, Validation, Data curation.



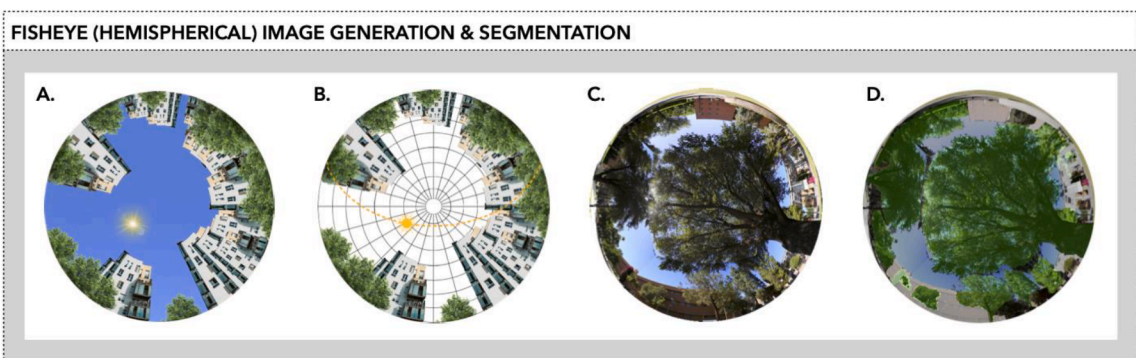


Fig. 6. Top: WebMRT user interface. Bottom: (A) Fisheye (hemispherical) image of a simulated built environment and exposure conditions, generated based on user-defined parameters; (B) Optional projection of sun trajectory; (C) Optional user-uploaded fisheye image; (D) Preview of segmentation results.

#### Declaration of competing interest

The authors declare the following financial interests/personal relationships which may be considered as potential competing interests:

Ariane Middel reports financial support was provided by National Science Foundation. If there are other authors, they declare that they have no known competing financial interests or personal relationships that could have appeared to influence the work reported in this paper.

#### Data availability

Data will be made available on request.

#### References

Agafonkin, V. (2023). SunCalc library [Computer software]. GitHub. https://github.

Bivand, R., Dokter, A. M., Huybrechts, P., Luque, S., Pelletier, G., & Tedeschi, A. (2023). suntools: Calculate sun position, sunrise, sunset, solar noon and twilight (p. version 1.0.0) [En]. GitHub. https://github.com/adokter/suntools/.

Bostock, M., Ogievetsky, V., & Heer, J. (2011). D<sup>3</sup> data-driven documents. *IEEE Transactions on Visualization and Computer Graphics*, 17(12), 2301–2309.

Breiman, L. (2001). Random forests. Machine Learning, 45(1), 5–32. https://doi.org/ 10.1023/A:1010933404324

Bruse, M., & Fleer, H. (1998). Simulating surface-plant-air interactions inside urban environments with a three dimensional numerical model. *Environmental Modelling & Software*, 13(3), 373–384. https://doi.org/10.1016/S1364-8152(98)00042-5

Buo, I., Sagris, V., Jaagus, J., & Middel, A. (2023). High-resolution thermal exposure and shade maps for cool corridor planning. Sustainable Cities and Society, 93, Article 104499.

Chapman, L., Thornes, J., & Bradley, A. (2001). Rapid determination of canyon geometry parameters for use in surface radiation budgets. *Theoretical and Applied Climatology*, 69, 81–89.

Chen, T., & Guestrin, C. (2016). Xgboost: A scalable tree boosting system. 785–794.
Clark, A. (2023). *Pillow: Vol. 9.0.0 [Computer software]*. Python Software Foundation. <a href="https://python-pillow.org">https://python-pillow.org</a>.

Crank, P. J., Middel, A., Wagner, M., Hoots, D., Smith, M., & Brazel, A. (2020). Validation of seasonal mean radiant temperature simulations in hot arid urban climates. Science of the Total Environment, 749, Article 141392.

Forouzandeh, A. (2018). Numerical modeling validation for the microclimate thermal condition of semi-closed courtyard spaces between buildings. *Sustainable Cities and Society*, 36, 327–345. https://doi.org/10.1016/j.scs.2017.07.025.

Gagge, A.P., Fobelets, A., & Berglund, L. (1986). A standard predictive index of human response to the thermal environment.

Gál, C. V., & Kántor, N. (2020). Modeling mean radiant temperature in outdoor spaces, A comparative numerical simulation and validation study. *Urban Climate*, 32, Article 100571.

- Guo, H., Aviv, D., Loyola, M., Teitelbaum, E., Houchois, N., & Meggers, F. (2020). On the understanding of the mean radiant temperature within both the indoor and outdoor environment, a critical review. Renewable and Sustainable Energy Reviews, 117, Article 109207.
- Guzman-Echavarria, G., Middel, A., & Vanos, J. (2023). Beyond heat exposure—New methods to quantify and link personal heat exposure, stress, and strain in diverse populations and climates: The journal temperature toolbox. *Temperature*, 10(3), 358–378.
- Hoerl, A. E., & Kennard, R. W. (1970). Ridge regression: Biased estimation for nonorthogonal problems. Technometrics: A Journal of Statistics for the Physical, Chemical, and Engineering Sciences, 12(1), 55–67.
- Höppe, P. (1999). The physiological equivalent temperature—a universal index for the biometeorological assessment of the thermal environment. *International Journal of Biometeorology*, 43(2), 71–75.
- Hughes, S., Giest, S., & Tozer, L. (2020). Accountability and data-driven urban climate governance. *Nature Climate Change*, 10(12), 1085–1090.
- [ IPCC. (2023). In H. Lee, & J. Romero (Eds.), Climate change 2023: Synthesis report. contribution of working groups I, II and III to the sixth assessment report of the intergovernmental panel on climate change (pp. 35–115). Core Writing TeamIPCC. https://doi.org/10.59327/IPCC/AR6-9789291691647 [(eds.)].
- James, G., Witten, D., Hastie, T., & Tibshirani, R. (2013). An introduction to statistical learning: With applications in R, 112. Springer.
- Jendritzky, G., de Dear, R., & Havenith, G. (2012). UTCI—Why another thermal index? International Journal of Biometeorology, 56, 421–428.
- Johansson, E., Thorsson, S., Emmanuel, R., & Krüger, E. (2014). Instruments and methods in outdoor thermal comfort studies—The need for standardization. *Urban Climate*. 10, 346–366.
- Kántor, N., & Unger, J. (2011). The most problematic variable in the course of human-biometeorological comfort assessment—The mean radiant temperature. *Central European Journal of Geosciences*, 3(1), 90–100. https://doi.org/10.2478/s13533-011-0010-x
- Ke, G., Meng, Q., Finley, T., Wang, T., Chen, W., Ma, W., et al. (2017). Lightgbm: A highly efficient gradient boosting decision tree. Advances in Neural Information Processing Systems, 30.
- Kirillov, A., Mintun, E., Ravi, N., Mao, H., Rolland, C., Gustafson, L., et al. (2023). Segment anything, 4015–4026.
- Kottek, M., Grieser, J., Beck, C., Rudolf, B., & Rubel, F. (2006). World Map of the Köppen-Geiger climate classification updated. *Meteorologische Zeitschrift*, 15(3), 259–263. https://doi.org/10.1127/0941-2948/2006/0130
- Krüger, E., Minella, F., & Matzarakis, A. (2014). Comparison of different methods of estimating the mean radiant temperature in outdoor thermal comfort studies. *International Journal of Biometeorology*, 58, 1727–1737.
- Lindberg, F., Holmer, B., & Thorsson, S. (2008). SOLWEIG 1.0 Modelling spatial variations of 3D radiant fluxes and mean radiant temperature in complex urban settings. *International Journal of Biometeorology*, 52(7), 697–713. https://doi.org/10.1007/s00484-008-0162-7
- Loh, W. (2011). Classification and regression trees. Wiley Interdisciplinary Reviews: Data Mining and Knowledge Discovery, 1(1), 14–23.
- Matzarakis, A., Rutz, F., & Mayer, H. (2007). Modelling radiation fluxes in simple and complex environments—Application of the RayMan model. *International Journal of Biometeorology*, 51(4), 323–334. https://doi.org/10.1007/s00484-006-0061-8

- Merchant, C., Meggers, F., Hou, M., Aviv, D., Schneider, F. A., & Middel, A. (2022). Resolving radiant: Combining spatially resolved longwave and shortwave measurements to improve the understanding of radiant heat flux reflections and heterogeneity. Frontiers in Sustainable Cities, 4, Article 869743.
- Middel, A., AlKhaled, S., Schneider, F. A., Hagen, B., & Coseo, P. (2021). 50 Grades of Shade. Bulletin of the American Meteorological Society, 102(9), E1805–E1820.
- Middel, A., AlKhaled, S., Schneider, F.A., Hagen, B., & Coseo, P. (forthcoming). MaRTy dataset—50 grades of shades project. DesignSafe-CI. </Dataset>.
- Middel, A., Huff, M., Krayenhoff, E. S., Udupa, A., & Schneider, F. A. (2023). PanoMRT: Panoramic infrared thermography to model human thermal exposure and comfort. Science of The Total Environment, 859, Article 160301.
- Middel, A., & Krayenhoff, E. S. (2019). Micrometeorological determinants of pedestrian thermal exposure during record-breaking heat in Tempe, Arizona: Introducing the MaRTy observational platform. Science of the Total Environment, 687, 137–151.
- Middel, A., Lukasczyk, J., & Maciejewski, R. (2017). Sky view factors from synthetic fisheye photos for thermal comfort routing-a case study in Phoenix, Arizona. *Urban Planning*, 2(1), 19–30. https://doi.org/10.17645/up.v2i1.855
- Middel, A., Lukasczyk, J., Zakrzewski, S., Arnold, M., & Maciejewski, R. (2019). Urban form and composition of street canyons: A human-centric big data and deep learning approach. *Landscape and Urban Planning*, 183, 122–132.
- Middel, A., Nazarian, N., Demuzere, M., & Bechtel, B. (2022). Urban climate informatics: An emerging research field. Frontiers in Environmental Science, 10, Article 867434.
- Pedregosa, F., Varoquaux, G., Gramfort, A., Michel, V., Thirion, B., Grisel, O., et al. (2011). Scikit-learn: Machine learning in Python. *The Journal of Machine Learning Research*, 12, 2825–2830.
- Rykaczewski, K., Joshi, A., Viswanathan, S. H., Guddanti, S. S., Sadeghi, K., Gupta, M., et al. (2024). A simple three-cylinder radiometer and low-speed anemometer to characterize human extreme heat exposure. *International Journal of Biometeorology*, 1–12
- Schneider, F. A., Epel, E., & Middel, A. (2024). A disconnect in science and practitioner perspectives on heat mitigation. Npj Urban Sustainability, 4(1), 17.
- Shashua-Bar, L., Pearlmutter, D., & Erell, E. (2011). The influence of trees and grass on outdoor thermal comfort in a hot-arid environment. *International Journal of Climatology*, 31(10), 1498–1506. https://doi.org/10.1002/joc.2177
- Smola, A. J., & Schölkopf, B. (2004). A tutorial on support vector regression. Statistics and Computing, 14, 199–222.
- Thorsson, S., Lindberg, F., Eliasson, I., & Holmer, B. (2007). Different methods for estimating the mean radiant temperature in an outdoor urban setting. *International Journal of Climatology*, 27(14), 1983–1993.
- Tibshirani, R. (1996). Regression shrinkage and selection via the lasso. *Journal of the Royal Statistical Society Series B: Statistical Methodology*, 58(1), 267–288.
- Vanos, J. K., Rykaczewski, K., Middel, A., Vecellio, D. J., Brown, R. D., & Gillespie, T. J. (2021). Improved methods for estimating mean radiant temperature in hot and sunny outdoor settings. *International Journal of Biometeorology*, 65(6), 967–983.
- Wu, R., Fang, X., Liu, S., & Middel, A. (2023). A fast and accurate mean radiant temperature model for courtyards: Evidence from the Keyuan Garden in central Guangdong, China. Building and Environment, 229, Article 109916.
- Zhao, T. F., & Fong, K. F. (2017). Characterization of different heat mitigation strategies in landscape to fight against heat island and improve thermal comfort in hot-humid climate (Part I): Measurement and modelling. Sustainable Cities and Society, 32, 523–531. https://doi.org/10.1016/j.scs.2017.03.025